A resilient and luminescent stimuli-responsive hydrogel from a heterotopic 1,8-naphthalimide-derived ligand

Chris S. Hawes,[a*] Amy D. Lynes[a], Kevin Byrne,[b] Wolfgang Schmitt,[b] Gavin Ryan,[c] Matthias E. Möbius[c] and Thorfinnur Gunnlaugsson[a*]

[a]*School of Chemistry and Trinity Biomedical Sciences Institute (TBSI), Trinity College Dublin, Dublin 2, Ireland. Email: hawescs@tcd.ie; gunnlaut@tcd.ie*

[b]*School of Chemistry and Centre for Research on Adaptive Nanostructures and Nanodevices (CRANN), Trinity College Dublin, Dublin 2, Ireland*

[c]*School of Physics, Trinity College Dublin, Dublin 2, Ireland*

Email: hawescs@tcd.ie; gunnlaut@tcd.ie

Supporting Information

Structure and Solvent Exchange Properties of *poly*-[CdL$_2$]

Colourless crystals of ***poly*-[CdL$_2$]** were analysed by single crystal X-ray diffraction, and a structural model was generated in the triclinic space group *P*-1, with the asymmetric unit containing one molecule of **L** deprotonated and coordinating to a Cd^{II} ion, as shown in Figure S1. The carboxylate group adopts a μ_2-κO:κO′ bridging coordination mode, with the cadmium ion exhibiting octahedral geometry with four carboxylate oxygen atoms in the equatorial plane and two equivalent pyridyl groups occupying the axial positions. The carboxylate bridging gives a well-ordered one-dimensional chain of cadmium ions, each separated by 4.6567(2) Å. These chains are linked into two-dimensional sheets parallel to the *ac* plane by **L** groups. The conformation of the ligands gives rectangular intra-layer channels walled by the inorganic chains and the buckled **L** groups, with minimum interatomic dimensions *ca*. 6.5 × 10 Å. Within each sheet the naphthalimide groups of each **L** ligand undergo head-to-head parallel π-π stacking interactions, with a mean interplanar distance of 3.41 Å. Adjacent layers pack closely by the symmetric undulating nature of the outer surfaces.

Thermogravimetric analysis of the as-synthesised material showed that thermal evacuation was not complete until *ca*. 200 °C, centred on an abrupt mass loss at 125 °C. The combination of thermogravimetric analysis and SQUEEZE volume and electron count[S1] suggest an occupancy of between 1 and 2 DMF molecules per **L** group in the freshly isolated material; elemental analysis after drying and standing in air revealed a formula of *poly*-[Cd**L**$_2$]·3.25H_2O for the dry sample, indicating exchange with atmospheric water. Soaking the freshly isolated material (***poly*-[CdL$_2$]{DMF}**, for clarity) in acetonitrile for 48 hours effected exchange of the lattice solvent molecules. This exchange also led to a reduction in crystallographic symmetry by single crystal X-ray diffraction. The model for the acetonitrile-exchanged material ***poly*-[CdL$_2$]{MeCN}** was best refined in a unit cell of almost double the original volume (2163 Å^3, *cf.* 1136 Å^3), with the asymmetric unit containing two **L** ligands and a single cadmium ion.

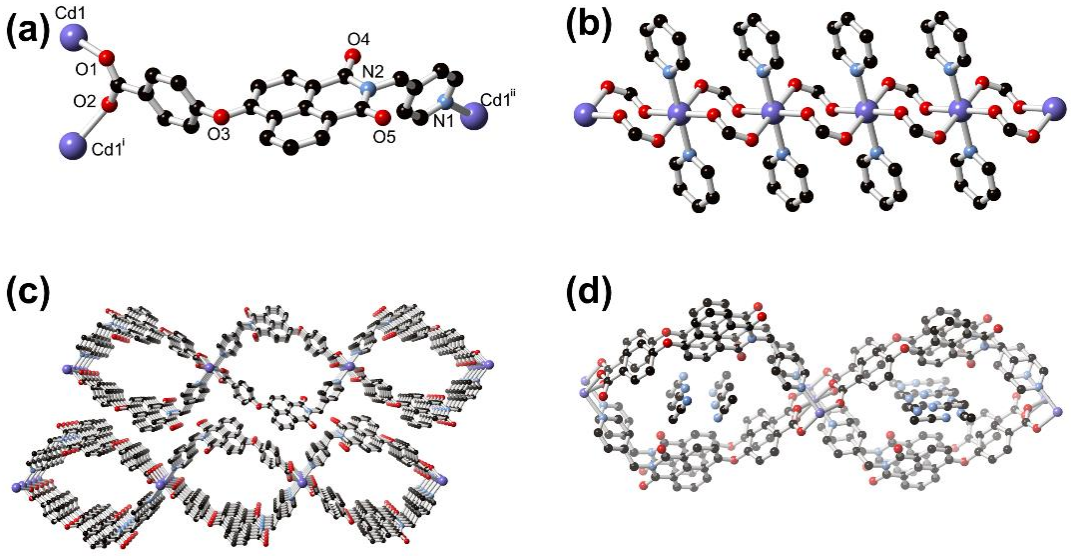

Figure S1 (a) The ligand environment in the structure of complex ***poly*-[CdL$_2$]** with heteroatom labelling scheme; (b) Coordination environment in the structure of ***poly*-[CdL$_2$]** showing the one-dimensional bridging motif of the cadmium ions; (c) Extended structure of ***poly*-[CdL$_2$]{DMF}** viewed parallel to the primary solvent channels; (d) Ordering of the lattice acetonitrile molecules within the solvent channels in ***poly*-[CdL$_2$]{MeCN}.** All hydrogen atoms are omitted for clarity. Symmetry codes to generate equivalent atoms: (i) 1+x, +y, +z; (ii) 1+x, +y, z-1.

Whereas no sensible discrete orientations for the guest solvent molecules could be detected for ***poly*-[CdL$_2$]{DMF}** (even when adopting the larger cell), in ***poly*-[CdL$_2$]{MeCN}** the position and orientation of the guest solvent molecules can be precisely determined. Two alternating, crystallographically unique intra-sheet channels are observed in ***poly*-[CdL$_2$]{MeCN}**; in the first of these channels, one fully-occupied acetonitrile site is present, with the guest species supported by C-H···N and C-H···O interactions with the naphthalimide walls (Figure S1/S2). In the other channel, crystallographic disorder is exhibited by the guest acetonitrile molecules which nonetheless display only two distinct orientations. The discrepancies in the orientation of the guest solvent molecules are accompanied by a conformational change in one of the two unique **L** molecules compared to the original structure, by a rotation of the picolyl group about the rotatable C-C and C-N bonds. Aside from the minor deviations in the conformation of the **L** units lining the channels, the bulk structure and interactions between adjacent layers remain unchanged between ***poly*-[CdL$_2$]{DMF}** and ***poly*-[CdL$_2$]{MeCN}.** The photoluminescence behaviour of both phases was probed; on irradiation at 366nm, both exhibit fluorescence with broad emission bands centered at 475 and 485nm, respectively; the minor red-shift of the emission band caused by replacing the lattice solvent molecules is smaller than that observed in the homoleptic dicarboxylate system.[S2]

The crystallographically determined formulation of the acetonitrile-exchanged material (*poly*-[Cd**L**$_2$]·1.5MeCN) was precisely corroborated by thermogravimetric analysis, with 5.6% mass loss by 100 °C (calculated 5.8%) followed by a broad plateau. Despite the mild conditions of activation afforded by the solvent exchange, after evacuation at 100 °C overnight the activated compound showed negligible uptake of N_2 at 77 K or CO_2 at 273 K (Figure S11/S12), consistent with an irreversible collapse of the primary channels following total evacuation.

Experimental

Materials and Methods

All reagents were used as received from commercial sources without further purification. *N*-(4-picolyl)-4-nitro-1,8-naphthalimide was prepared according to the previously reported procedure.[S3] NMR spectra were recorded using a Bruker AVANCE III instrument operating at 400 MHz for ^{1}H and 100 MHz for ^{13}C. Chemical shifts are reported in ppm with the residual solvent as the internal reference. All NMR spectra were carried out at 293 K. Mass spectra were acquired using a Micromass time of flight mass spectrometer (tof), interfaced to a Waters 2690 HPLC. The instrument was operated in positive or negative mode as required. Leucine Enkephalin was used as an internal lock mass. Masses were recorded over the range 100-1000 m/z. Melting points were determined using an Electrothermal IA9000 digital melting point apparatus and are uncorrected. Infrared spectra were recorded on a PerkinElmer Spectrum One FTIR spectrometer in the range 4000 - 550 cm^{-1}. Thermogravimetric analysis was performed on Perkin Elmer Pyris 1 TGA in the temperature range 25-500 °C with a scan rate 5 °C min^{-1} under a nitrogen atmosphere with N_2 flow rate 20 mL/min. X-ray powder diffraction patterns were recorded with a Bruker D2 Phaser instrument using Cu-Kα (λ = 1.5405 Å) radiation at room temperature. Raw data were compared with the simulated patterns from the single crystal data collections carried out at 100 K. Rheological measurements were carried out with an Anton Paar MCR 301 rheometer using a plate-plate geometry. All measurements were carried out in duplicate to ensure reproducibility. All photophysical measurements were performed at 298K in either spectroscopic grade dimethyl sulfoxide or Milli-Q water. UV-Vis absorption spectra were measured in 1 cm quartz cuvettes on a Varian Cary 50 spectrophotometer. Fluorescence spectra were measured on a Varian Cary Eclipse Fluorimeter. Quantum yields were calculated by comparison with quinine sulfate in 2M H_2SO_4 with excitation at 366nm using an excitation slit width of 2.5nm for all samples, and emission integrated across the range 380 – 600nm. Solid-state emission spectra were measured at room temperature with powdered samples pressed into films between quartz plates. Gas adsorption isotherms were measured using a using a Quantachrome Autosorb IQ gas sorption analyser. Chemically pure (CP, N4.5) grade He, N_2 and CO_2 gases from BOC gases were used for the measurements. The sample was de-gassed under dynamic vacuum at 100 °C for 24 hours prior to the measurements. SEM images were collected with a Carl Zeiss Ultra SEM, with the samples deposited on silicon wafers with a thick silicon dioxide layer. Prior to imaging, all samples were coated with a conductive layer of Pd/Au using a Cressington 208Hr high resolution sputter coater.

Synthesis of *N*-(4-picolyl)-4-(4′-carboxyphenoxy)-1,8-naphthalimide HL

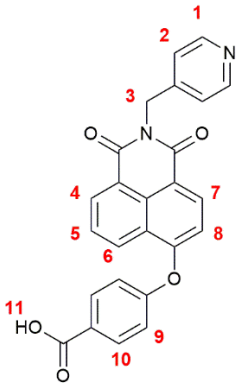

N-(4-picolyl)-4-nitro-1,8-naphthalimide (200 mg, 0.6 mmol), 4-hydroxybenzoic acid (160 mg, 1.2 mmol) and potassium carbonate (240 mg, 1.8 mmol) were combined in 5 mL of anhydrous DMSO and the mixture was heated under argon at 120 °C for 3 hours. The mixture was cooled to room temperature, and 5 mL of 1:1 MeOH:HOAc was added dropwise, causing precipitation of a tan solid. The solid was filtered and washed sequentially with methanol (20 mL), water (20 mL) and methanol (20 mL), and dried in air. Yield 184 mg (73%). m.p. > 300°C; Found C, 68.49; H, 3.75; N, 6.38; calculated for $C_{25}H_{16}N_2O_5 \cdot 0.66H_2O$ C, 68.80; H, 4.00; N, 6.42%; δ_H (400MHz, d_6-DMSO) 5.28 (s, 2H, H^3), 7.25 (d, 1H, J = 8.3 Hz, H^8), 7.31 – 7.37 (m, 4H, $H^9 + H^2$), 7.95 (dd, 1H, J = 8.3, 7.5 Hz, H^5), 8.07 (d, 2H, J = 8.7 Hz, H^{10}), 8.47 – 8.51 (m, 3H, $H^7 + H^1$), 8.61 (d, 1H, J = 7.2 Hz, H^4), 8.66 (d, 1H, J = 8.3 Hz, H^6), 13.0 (br s, 1H, H^{11}); δ_C (100 MHz, d_6-DMSO) 42.20, 113.38, 117.18,

119.65, 122.19, 123.83, 127.54, 128.47, 129.32, 131.99, 132.92, 134.04, 146.24, 149.63, 157.81, 158.87, 162.89, 163.05, 163.55, 166.55; ν_{max}(ATR, cm^{-1}) 3074w, 2784w, 2484w br, 1694s br, 1652s, 1593m sh, 1501m, 1468w, 1415m, 1387s, 1352s, 1315s, 1278s, 1240s sh, 1151w, 1125m, 1093w, 1015m, 986w, 871m, 846m, 779s, 757m, 702m; *m/z* (ESI) 425.1134 ($[M+H]^+$, calculated for $C_{25}H_{17}N_2O_5$ 425.1137; 423.1000 ($[M-H]^-$, calculated for $C_{25}H_{15}N_2O_5$ 423.0981; λ_{max}/nm (ε/ $L \cdot mol^{-1} \cdot cm^{-1}$) 360 (14300 ± 600)

Synthesis of gel 1 (10 mg/mL, residual 3.3 wt%)

Ligand **HL** (10 mg; 24 μmol) was dispersed in 500 μL of water with the aid of sonication. To this mixture was added a solution of potassium carbonate (20 mg; 140 μmol) in 500 μL of water. The resulting mixture was heated with shaking until a clear homogenous solution resulted. Upon cooling to room temperature the gel set completely within several minutes. This method was scaled linearly to generate larger quantities of the gel, up to 10 mL for rheology measurements. Equivalent procedures were used to generate the gels at other concentrations and L:K_2CO_3 ratios.

Synthesis of *poly*-[CdL_2]

Ligand **HL** (10 mg, 24 μmol) and cadmium chloride tetrahydrate (7 mg, 27 μmol) were combined in 1 mL of a 95:5 DMF:H_2O mixture. The mixture was sonicated briefly and sealed in a glass vial and heated to 100 °C. After 48 hours at this temperature, the resulting pale yellow crystals were filtered hot, washed with DMF and dried in air. Yield 5.4 mg (44%). Thermogravimetric analysis of a freshly isolated sample showed a total of *ca.* 20% volatile mass, consistent with approximately 3 DMF molecules, 10 water molecules, or a combination, per cadmium ion (including contribution from the crystal surfaces).The best approximation for the lattice solvation in the air-dried sample approximately 2 weeks after isolation was estimated by microanalysis at 3.25 water molecules per cadmium ion. m.p. > 300°C Found C, 58.86; H, 2.97; N, 5.44; calculated for $C_{50}H_{30}N_4O_{10}Cd \cdot 3.25H_2O$ C, 59.00; H, 3.62; N, 5.51%; ν_{max}(ATR, cm^{-1}) 3059w, 2998w, 2928w, 1695m, 1655s sh, 1614w, 1595s, 1579m, 1555s, 1509w, 1494m, 1465m, 1425w, 1381s, 1346s, 1308m, 1241s sh, 1206m, 1180m, 1151m, 1134m, 1090m br, 1070m, 1014s, 993m, 948w, 872m, 857m, 835m sh, 803m, 779s sh, 753m, 709m, 659m sh, 609m, 579m,.

Conversion of *poly*-[CdL_2]{DMF} to *poly*-[CdL_2]{MeCN}

Crystals of ***poly*-[CdL_2]{DMF}** (*ca.* 10 mg) were directly transferred from the reaction solution into 10 mL of fresh DMF, allowed to stand for 2 hours, and then transferred into 20 mL of acetonitrile and sealed. The mixture was allowed to stand for 48 hours, and the solvent decanted and replaced every 12 hours with fresh acetonitrile without allowing the crystals to dry. ν_{max}(ATR, cm^{-1}) 3064w, 2937w, 2250w, 1698s, 1658s, 1615w, 1595s, 1579m, 1557s, 1512m, 1495m, 1467m, 1427w, 1383s sh, 1356s sh, 1241s sh, 1208m, 1182m, 1150m, 1135m, 1088w, 1070m, 1040w, 1015m, 991m, 946m, 885w, 870m, 855m, 782s, 753m, 707m, 649m, 611w, 580s.

X-ray Crystallography

Structural and refinement parameters are presented in Table S1. All diffraction data were collected using a Bruker APEX-II Duo dual-source instrument using Mo Kα (λ = 0.71073 Å) (***poly*-[CdL$_2$]{DMF}**) or microfocus Cu Kα (λ = 1.54178 Å) radiation (***poly*-[CdL$_2$]{MeCN}**,). Datasets were collected using ω and φ scans with the samples immersed in oil and maintained at a constant temperature of 100 K using a Cobra cryostream. The data were reduced and processed using the Bruker APEX suite of programs.[S4] Multi-scan absorption corrections were applied using SADABS.[S5] The diffraction data were solved using SHELXT and refined by full-matrix least squares procedures using SHELXL-2015 within the OLEX-2 GUI.[S6-S8] The functions minimized were $\Sigma w(F^2_o-F^2_c)$, with $w=[\sigma^2(F^2_o)+aP^2+bP]^{-1}$, where $P=[\max(F_o)^2+2F^2_c]/3$. All non-hydrogen atoms were refined with anisotropic displacement parameters. All hydrogen atoms were placed in calculated positions and refined with a riding model, with isotropic displacement parameters equal to either 1.2 or 1.5 times the isotropic equivalent of their carrier atoms. Specific refinement strategies are outlined in the combined crystallographic information file (cif).

In the case of complex ***poly*-[CdL$_2$]{DMF}**, the residual electron density relating to the lattice solvent molecules could not realistically be resolved into discrete atom sites, and was treated with the SQUEEZE routine within PLATON.[S1] The residual electron count (59 electrons per cadmium ion, 194 Å^3) are consistent with a void occupancy of between 1 and 2 DMF molecules per cadmium ion (40 or 80 electrons respectively, with density of between 40 and 20 Å^3 per non-hydrogen atom). Elemental analysis and TGA both indicated that this volatile mass was exchangeable for atmospheric water on standing in air.

In the case of complex ***poly*-[CdL$_2$]{MeCN}**, a near-doubling of the unit cell volume for the most reasonable model was observed compared to **1**. While ***poly*-[CdL$_2$]{DMF}** could also be indexed with the unit cell for ***poly*-[CdL$_2$]{MeCN}** input, this refinement exhibited large correlation elements between equivalent atoms, unreasonable U_{ij} tensors, no improvement in localisation of the lattice solvent molecules, and the two **L** units were geometrically equivalent and related by translational symmetry. Conversely, in ***poly*-[CdL$_2$]{MeCN}**, a clear distinction can be drawn between the geometry of the two unique **L** units, and the lattice acetonitrile molecules can be clearly resolved using minimal geometric restraints. Forced indexation of ***poly*-[CdL$_2$]{MeCN}** with the unit cell setting for ***poly*-[CdL$_2$]{DMF}** results in a highly disordered and poor quality structural model. A comparison of the solvent channel volume for ***poly*-[CdL$_2$]{DMF}** and ***poly*-[CdL$_2$]{MeCN}**is shown in Figure S2.

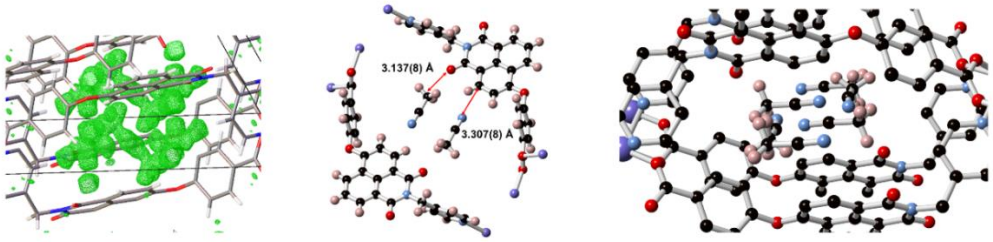

Figure S2 Comparison of the pore contents of ***poly*-[CdL$_2$]{DMF}** and ***poly*-[CdL$_2$]{MeCN}:** (Left) 3-dimensional Fourier difference map of the disordered solvent channel contents of ***poly*-[CdL$_2$]{DMF}** ($F^2_o-F^2_c$ positive values in green, rendered at 0.6 e·Å^{-3}); (Middle) Orientation and C-H···O/N interactions between the framework and well-ordered acetonitrile molecules within the ordered channel of ***poly*-[CdL$_2$]{MeCN}**; (Right) Two overlapping orientations of lattice acetonitrile molecules within the disordered channel of ***poly*-[CdL$_2$]{MeCN}**. Each molecule is modelled at 0.25 occupancy.

Table S1 Crystal and refinement parameters for complexes ***poly*-[CdL]{DMF}** and ***poly*-[CdL]{MeCN}**

Identification code	***poly*-[CdL]{DMF}**	***poly*-[CdL]{MeCN}**
Empirical formula	$C_{50}H_{30}CdN_4O_{10}$	$C_{53}H_{34.5}CdN_{5.5}O_{10}$
Formula weight	959.18	1020.76
Temperature/K	100	100.01
Crystal system	triclinic	triclinic
Space group	*P*-1	*P*-1
a/Å	4.6567(2)	4.57350(10)
b/Å	15.5275(5)	17.4178(4)
c/Å	17.3063(6)	27.7382(7)
α/°	66.4860(10)	101.062(2)
β/°	85.011(2)	93.619(2)
γ/°	82.452(2)	90.377(2)
Volume/Å^3	1136.69(7)	2163.86(9)
Z	1	2
ρ_{calc}g/cm^3	1.401	1.567
μ/mm^{-1}	0.543	4.647
F(000)	486	1038
Crystal size/mm^3	0.20 × 0.10 × 0.04	0.11 × 0.09 × 0.04
Radiation	Mo Kα (λ = 0.71073)	Cu Kα (λ = 1.54178)
2Θ range for data collection/°	3.012 to 61.232	3.252 to 136.744
Index ranges	$-6 \le h \le 6$, $-22 \le k \le 22$, $-24 \le l \le 24$	$-5 \le h \le 5$, $-21 \le k \le 20$, $-33 \le l \le 33$
Reflections collected	34854	26766
Independent reflections	7012 [R_{int} = 0.0700, R_{sigma} = 0.0627]	7888 [R_{int} = 0.0460, R_{sigma} = 0.0433]
Reflections Observed [I>=2σ (I)]	5788	7072
Data/restraints/parameters	7012/0/295	7888/76/668
Goodness-of-fit on F^2	1.033	1.052
Final R indexes [I>=2σ (I)]	R_1 = 0.0427, wR_2 = 0.0852	R_1 = 0.0539, wR_2 = 0.1359
Final R indexes [all data]	R_1 = 0.0601, wR_2 = 0.0896	R_1 = 0.0599, wR_2 = 0.1407
Largest diff. peak/hole / e Å^{-3}	0.90/-1.24	2.52/-0.75
CCDC Number	1540593	1540594

Additional SEM Images and Rheology Plots

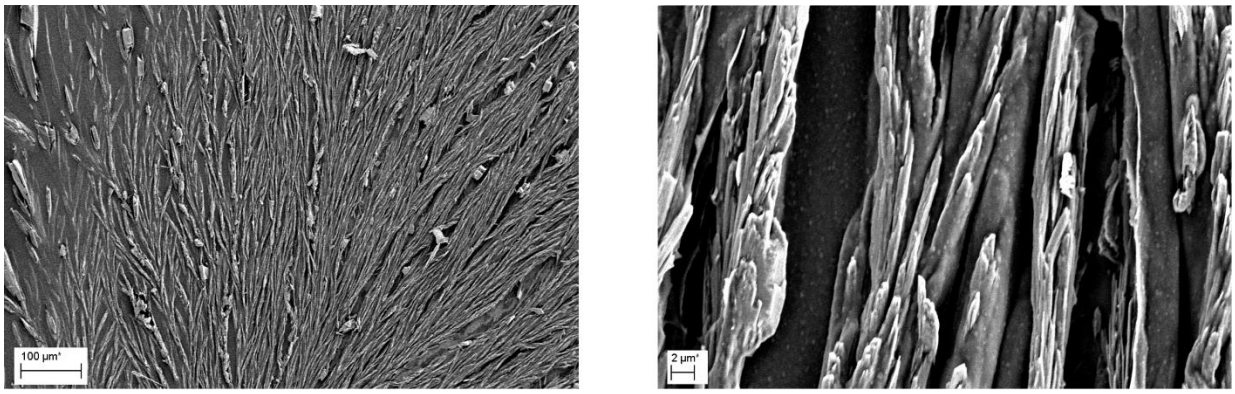

Figure S3 Additional SEM images prepared by smearing gel **1** onto a silicon plate and drying under dynamic vacuum, showing the fibrous nature of the xerogel . Scalebars 100µm (left) and 2 µm (right).

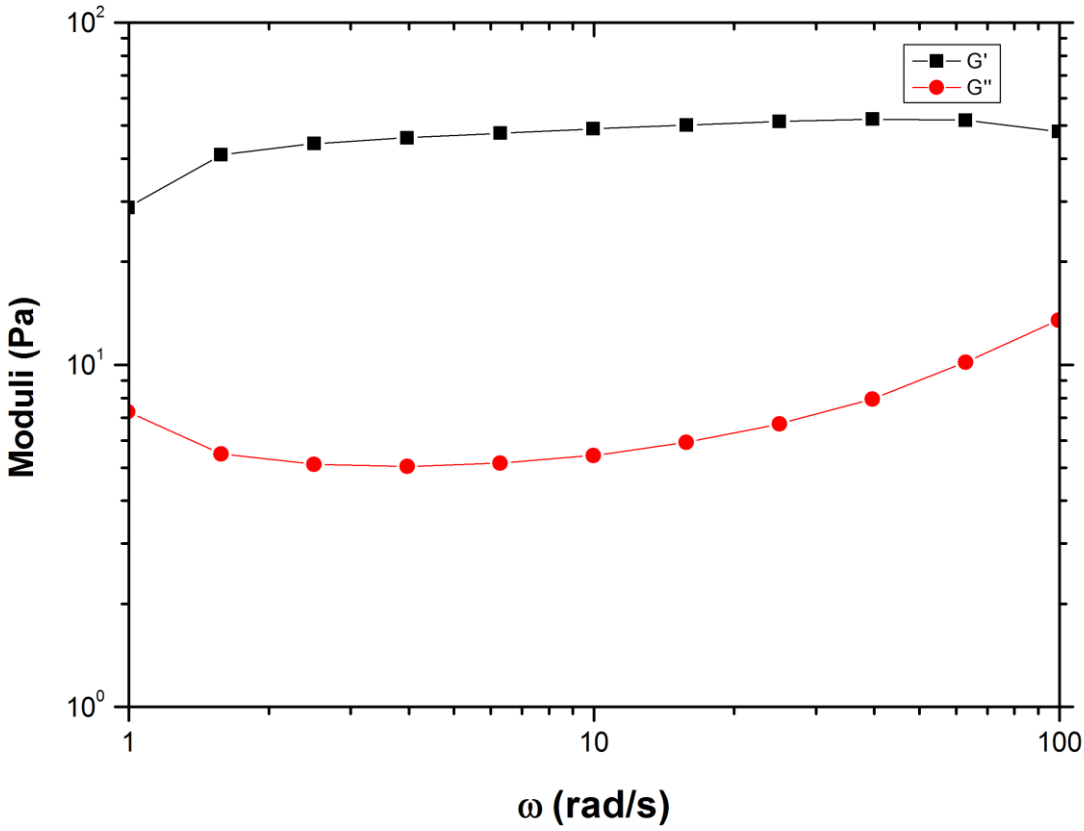

Figure S4 Frequency sweep rheological experiment for gel **1** ($\gamma = 0.1\%$)

Thermogravimetric Analysis

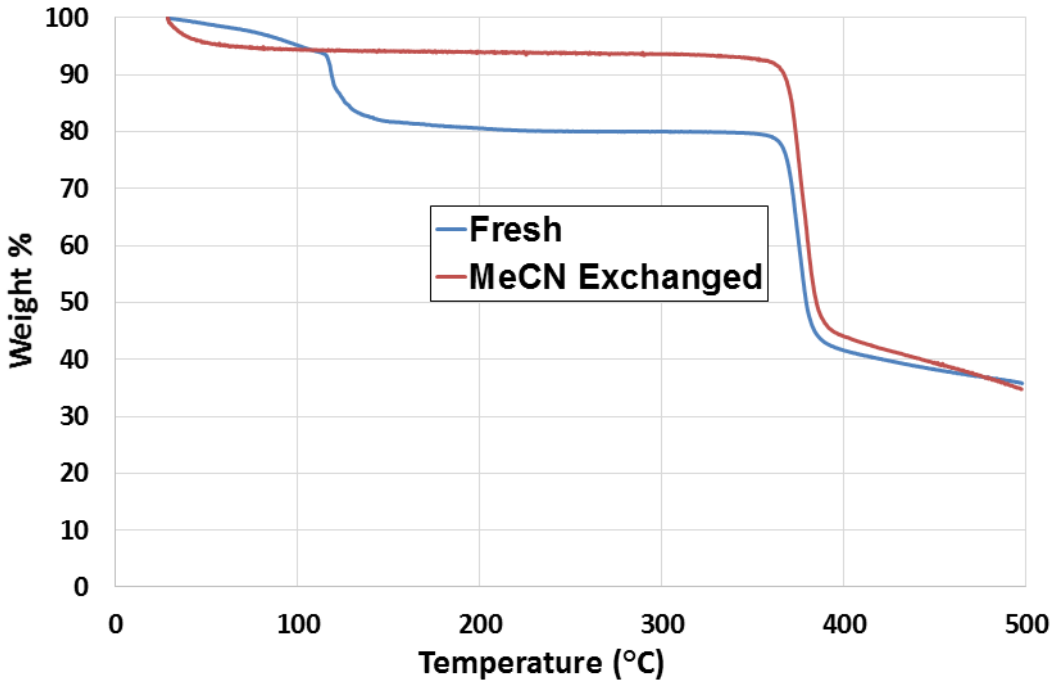

Figure S5 Thermogravimetric analysis plot of ***poly*-[CdL$_2$]{DMF}** (blue) and ***poly*-[CdL$_2$]{MeCN}** (red)

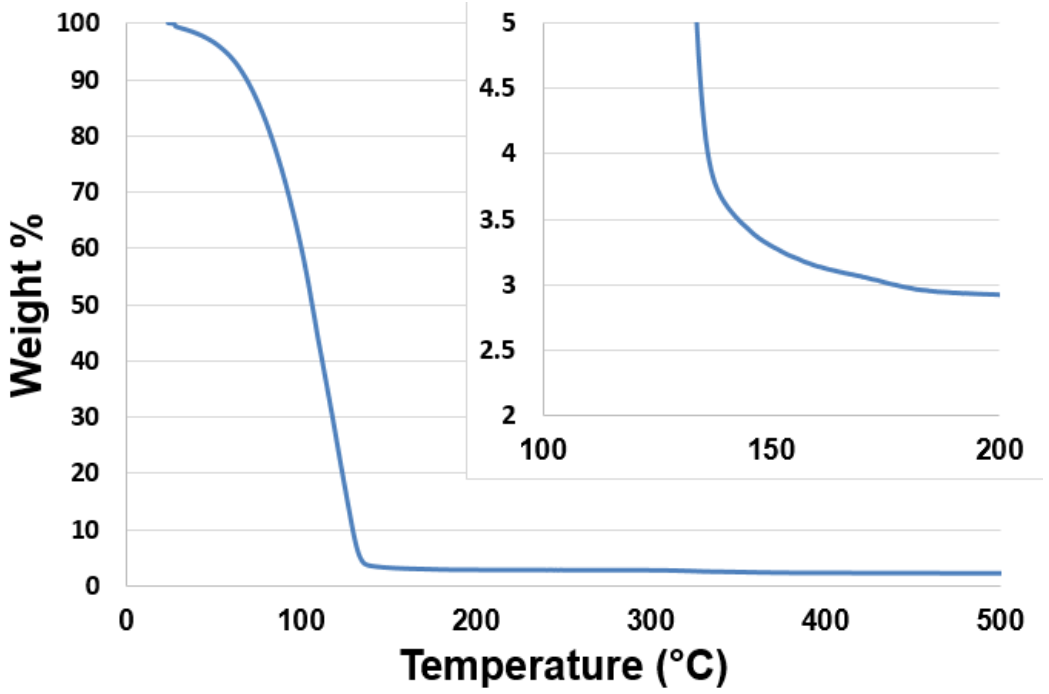

Figure S6 Thermogravimetric analysis for gel **1** (10 mg/mL, residual 3.3 wt%), with enlargement of the desolvation region (inset)

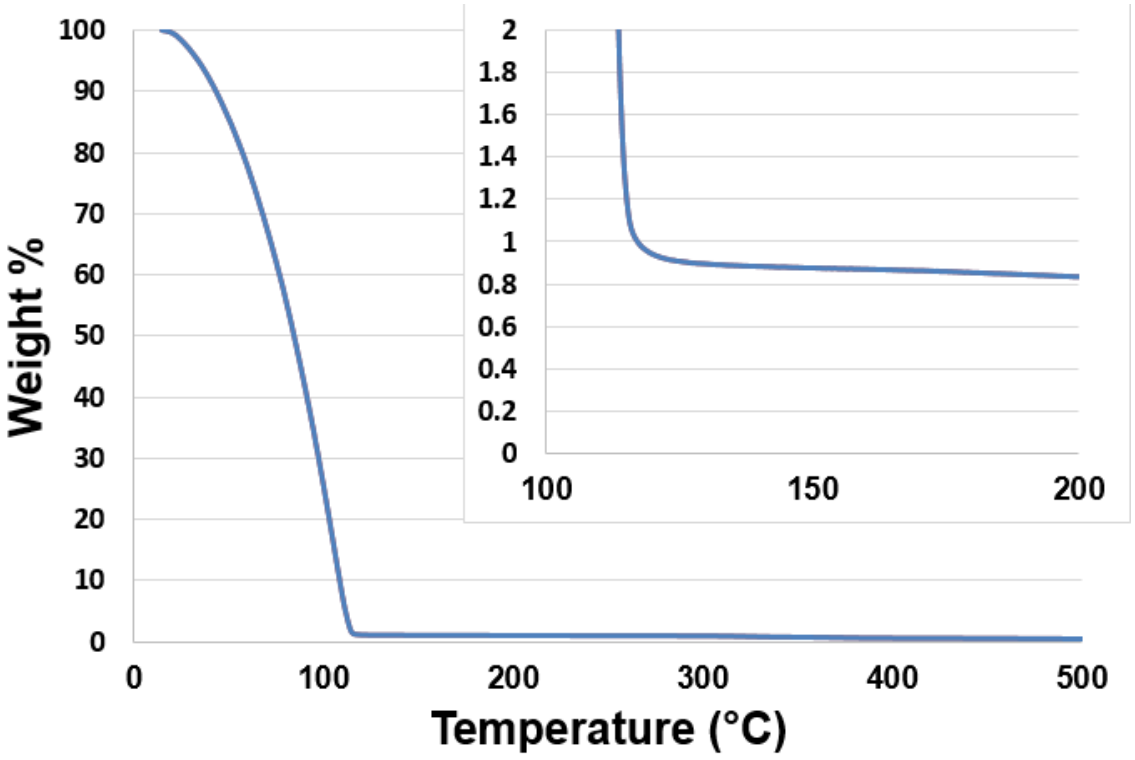

Figure S7 Thermogravimetric analysis for gel **1** (5 mg/mL, residual 0.9 wt%), with enlargement of the desolvation region (inset)

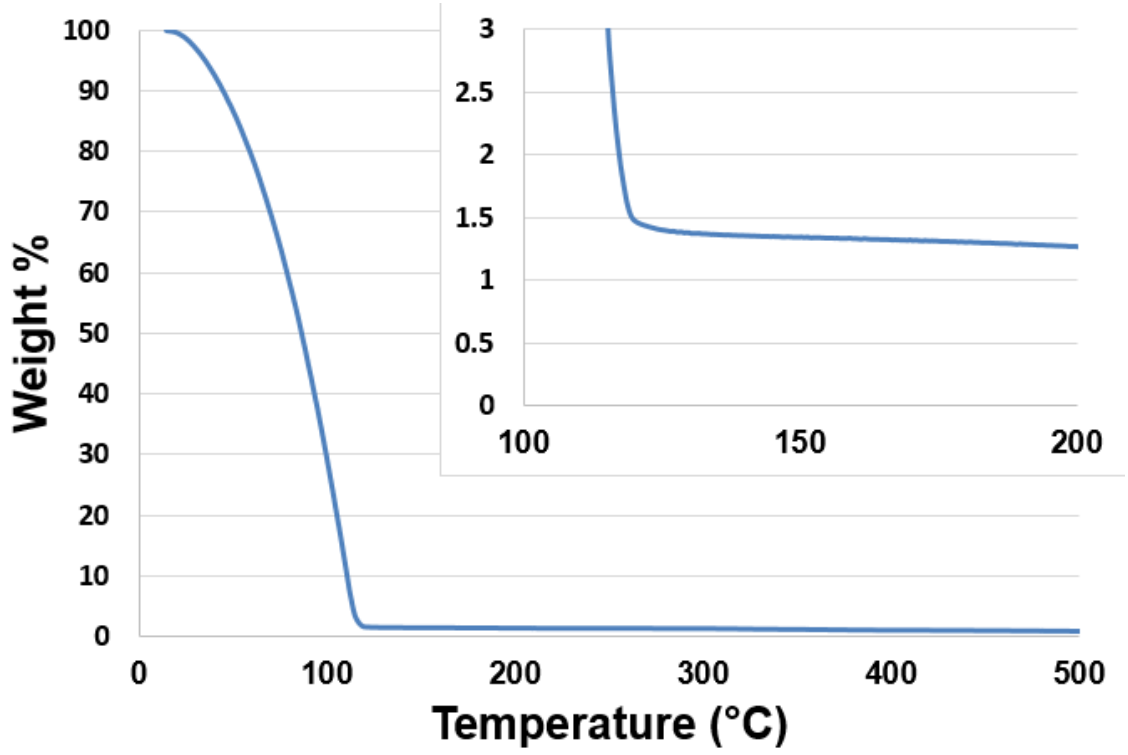

Figure S8 Thermogravimetric analysis for gel **1** (2.5 mg/mL, residual 1.3 wt%), with enlargement of the desolvation region (inset).

X-ray Powder Diffraction

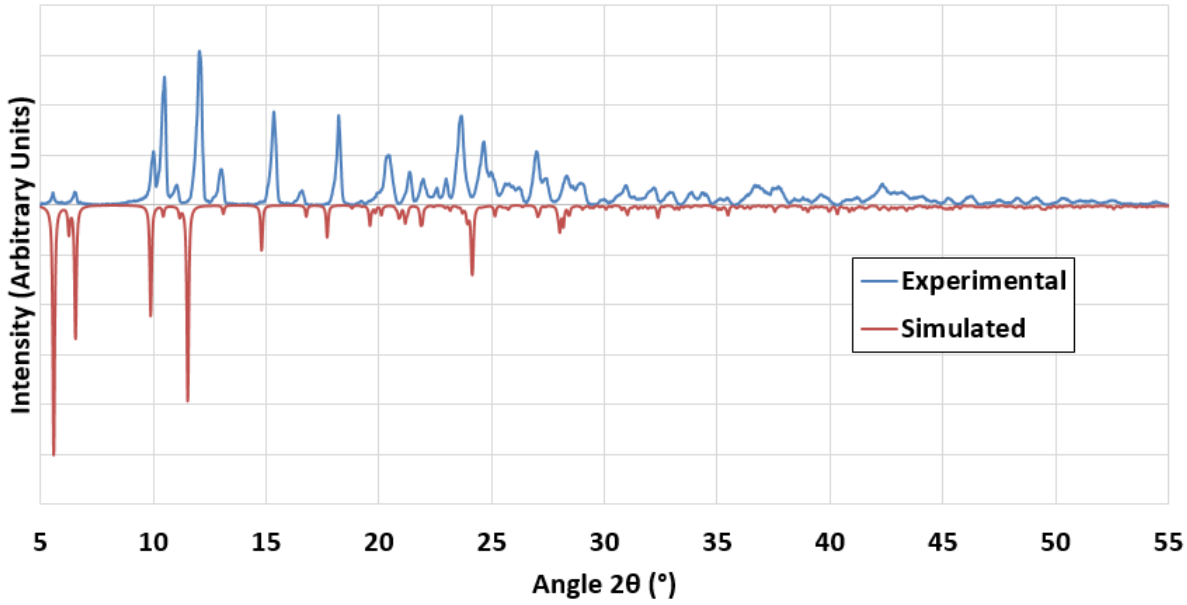

Figure S9 X-ray powder diffraction pattern for complex ***poly*-[CdL$_2$]{DMF}**, measured at room temperature (blue), compared with the pattern simulated from the single crystal diffraction data measured at 100K (red).

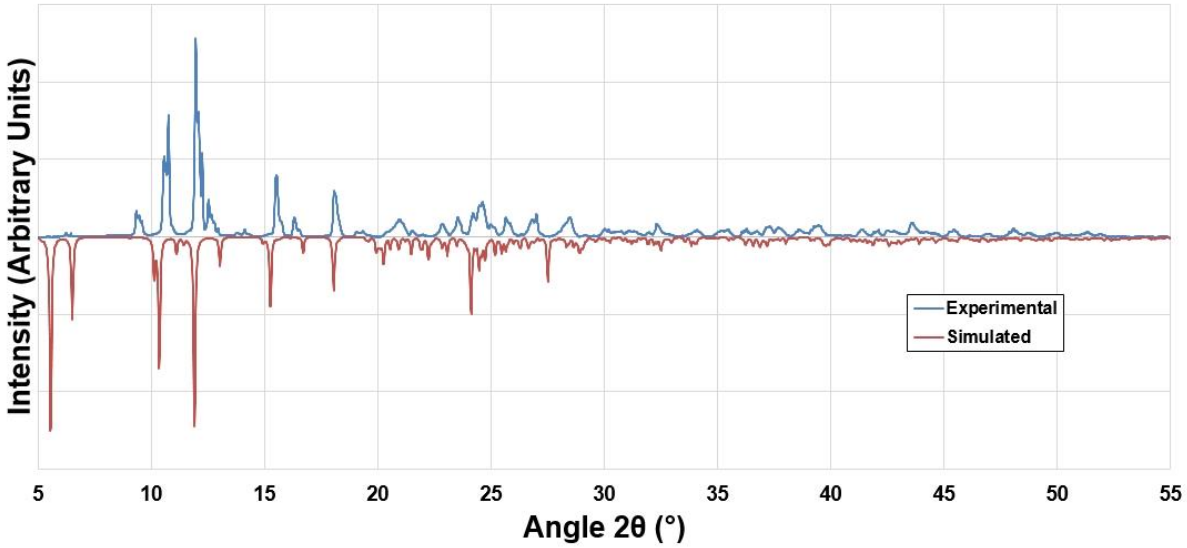

Figure S10 X-ray powder diffraction pattern for ***poly*-[CdL$_2$]{MeCN}** (blue) recorded at room temperature, and comparison with the data simulated from the single crystal data measured at 100K (red).

Gas Adsorption Isotherms

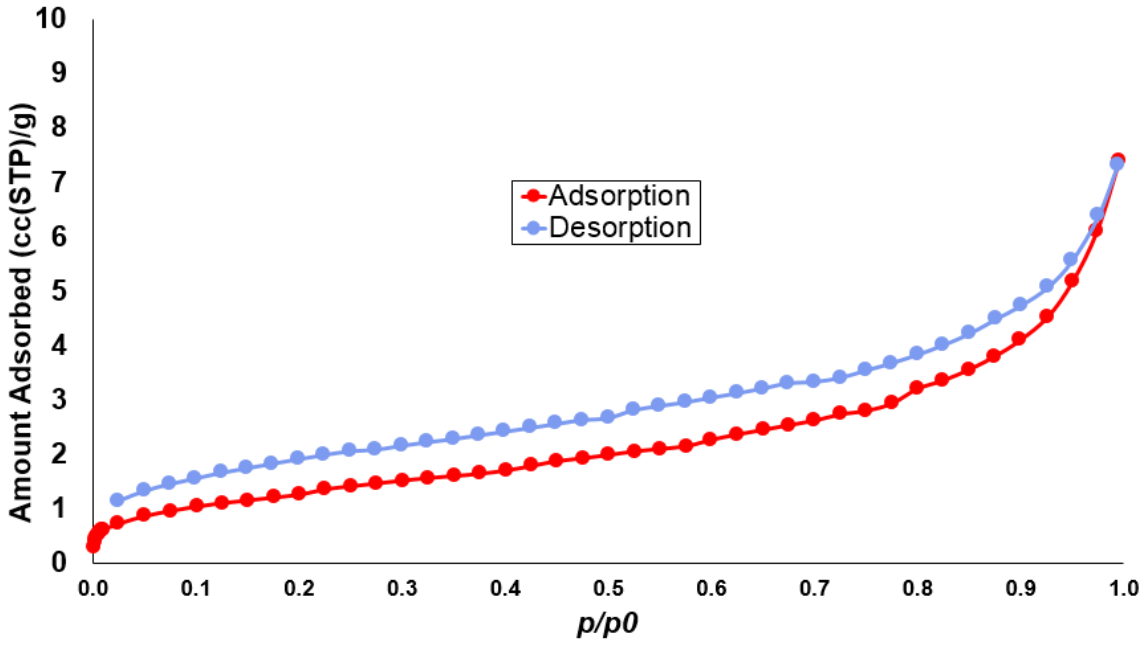

Figure S11 N_2 adsorption isotherm for ***poly*-[CdL$_2$]{MeCN}** at 77K after evacuation, showing negligible uptake of N_2. We ascribe the adsorption in the region p/p_0 = 0.8 – 0.99 to mesoporous defects or crystallite boundaries formed during the activation process.

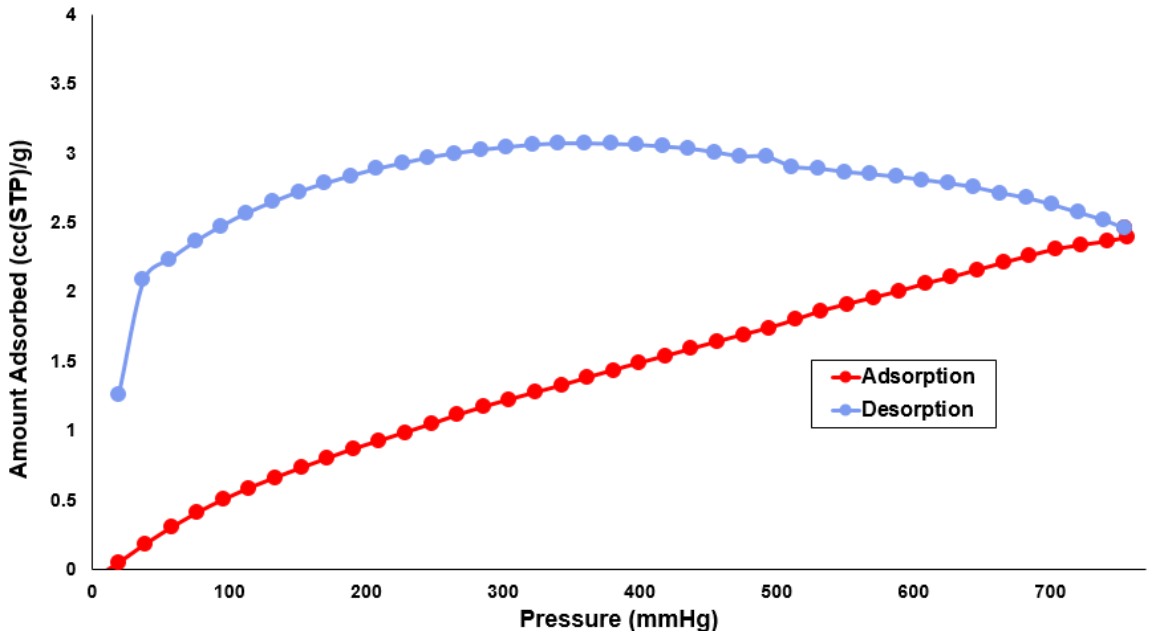

Figure S12 CO_2 adsorption isotherm for ***poly*-[CdL$_2$]{MeCN}** at 273K after evacuation, showing essentially negligible uptake of CO_2, and slight hysteresis on the desorption branch due to slow uptake kinetics.

UV-Visible and Fluorescence Spectroscopy

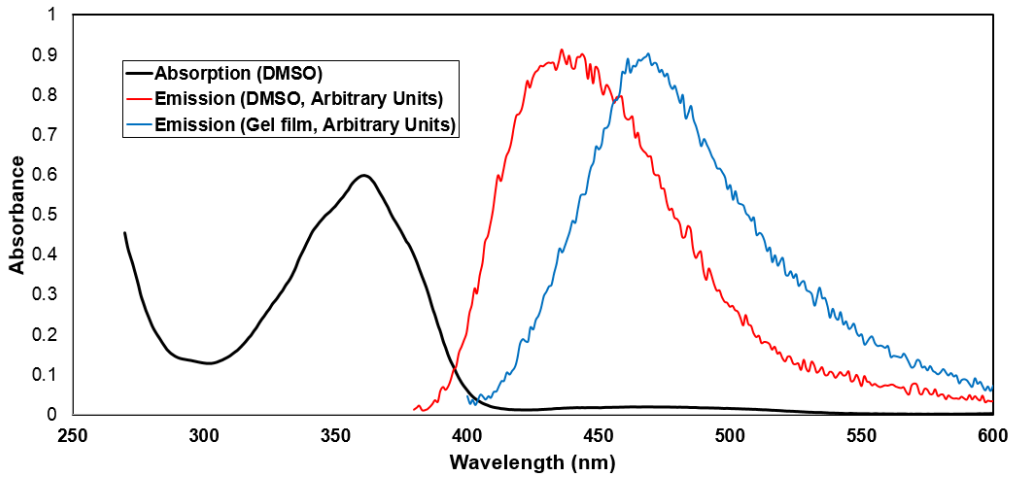

Figure S13 Absorption (black) and emission (red, λ_{ex} = 366nm) spectrum of **HL** in DMSO (40 μM), and emission spectrum of a film of gel **1** (λ_{ex} = 366nm)

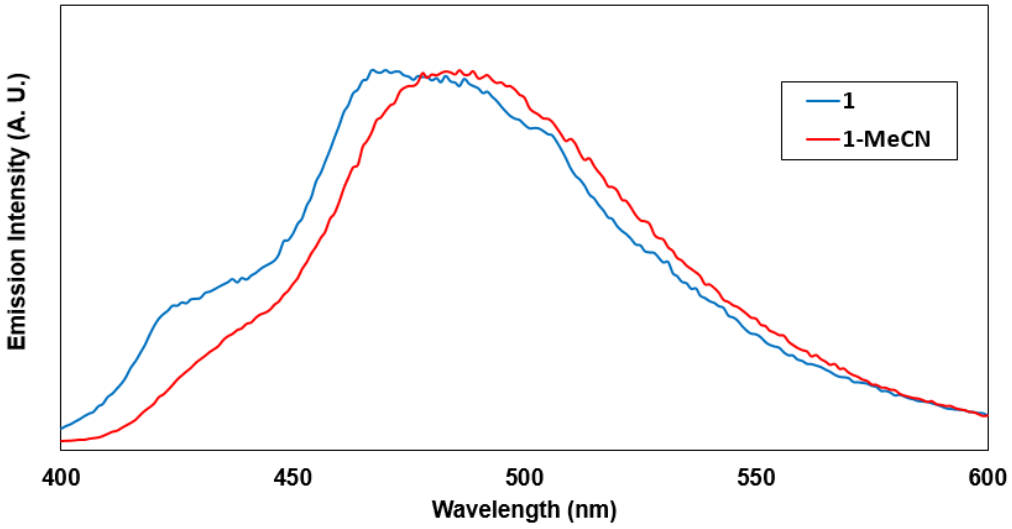

Figure S14 Comparison of the solid-state emission spectra of ***poly*-[CdL$_2$]{MeCN}** (blue) and ***poly*-[CdL$_2$]{DMF}** (red), with λ_{ex} = 366nm for both samples.

Quantum Yield Determination for HL

The photoluminescence quantum yield of **HL** was determined using a comparative method[S9] with quinine sulfate in 2M H_2SO_4 as a reference standard (Φ_F = 0.546, λ_{ex} = 366nm).[S10] The absorbance (366nm) and integrated emission (380 – 600 nm, excitation slit 2.5nm) of the standard and unknown solutions were measured across a range of concentrations and plotted (Figure S15), and the quantum yield Φ of the unknown solution was determined by the relation

$$\Phi_{unknown} = \Phi_{standard}(Grad_{unknown}/Grad_{standard})(\eta^2_{standard}/\eta^2_{unknown})$$

Where η is the refractive index of each solvent and Grad is the gradient of the best fit line for absorbance *versus* integrated emission. Each series of measurements was repeated in triplicate. Due to the low quantum yield of **HL** compared to the best available reference standard, the true uncertainty is expected to be larger than the sum of the measurement uncertainties, and of a similar order of magnitude as the value itself, and as such the value of Φ ~ 0.02 given is an approximation only.

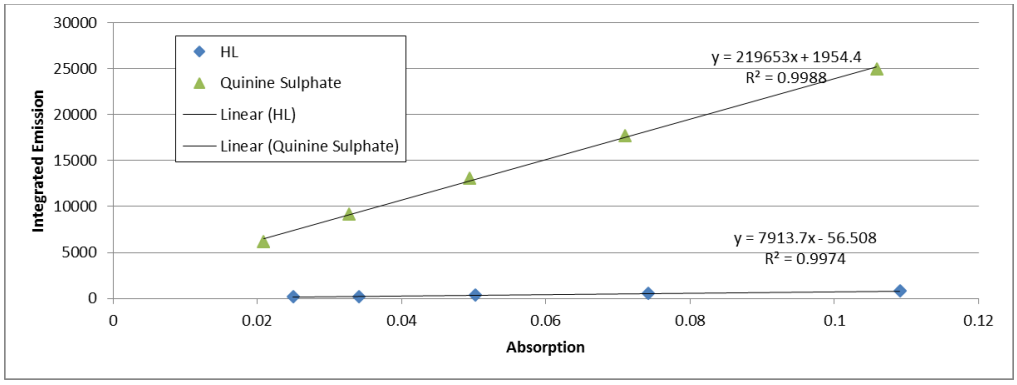

Figure S15 Comparison of integrated emission *vs* absorbance for **HL** and quinine sulphate reference standard.

NMR Spectroscopy

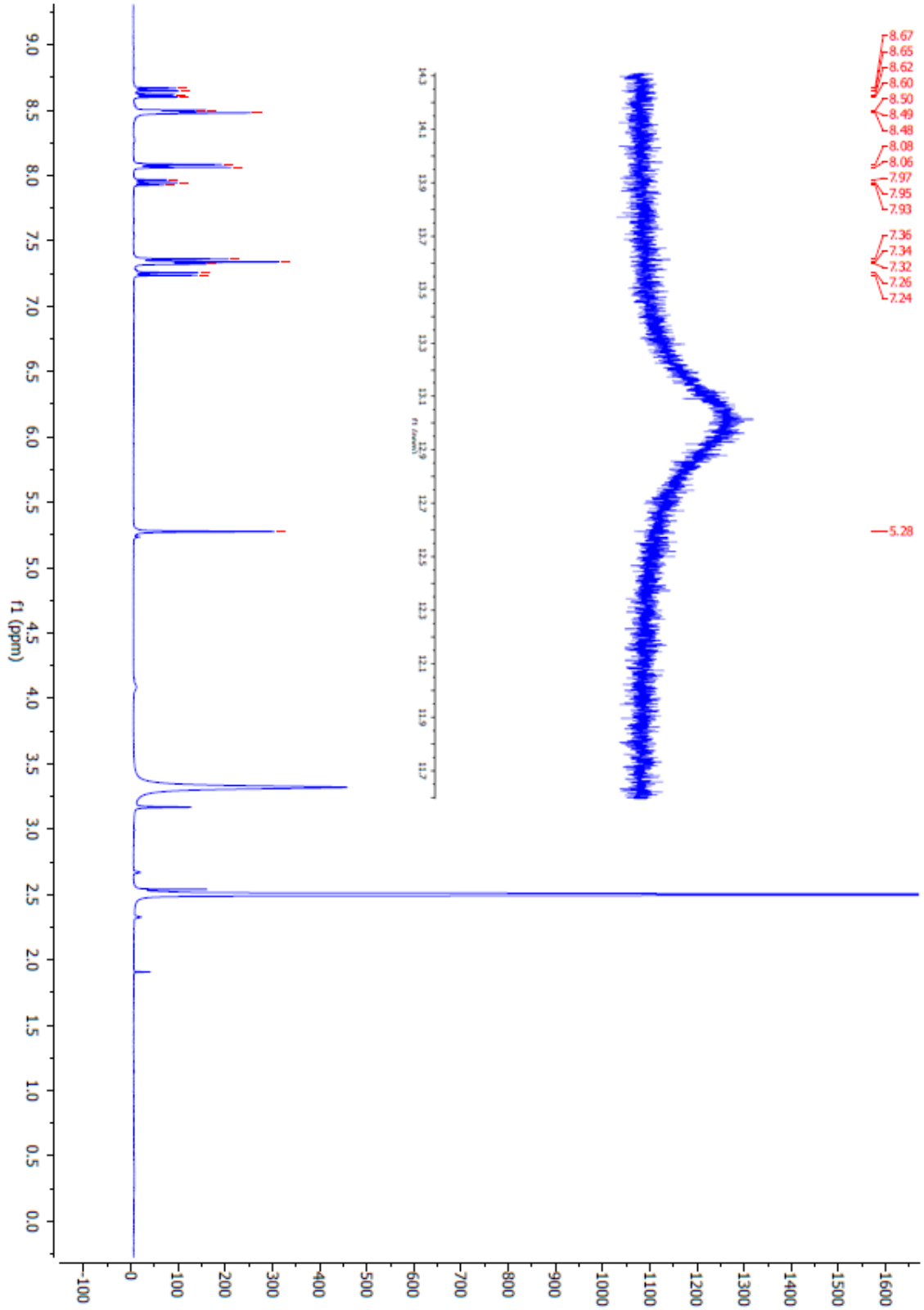

Figure S16 ^{1}H NMR spectrum of **HL** (400 MHz, d_6-DMSO) with broad carboxylic acid resonance inset.

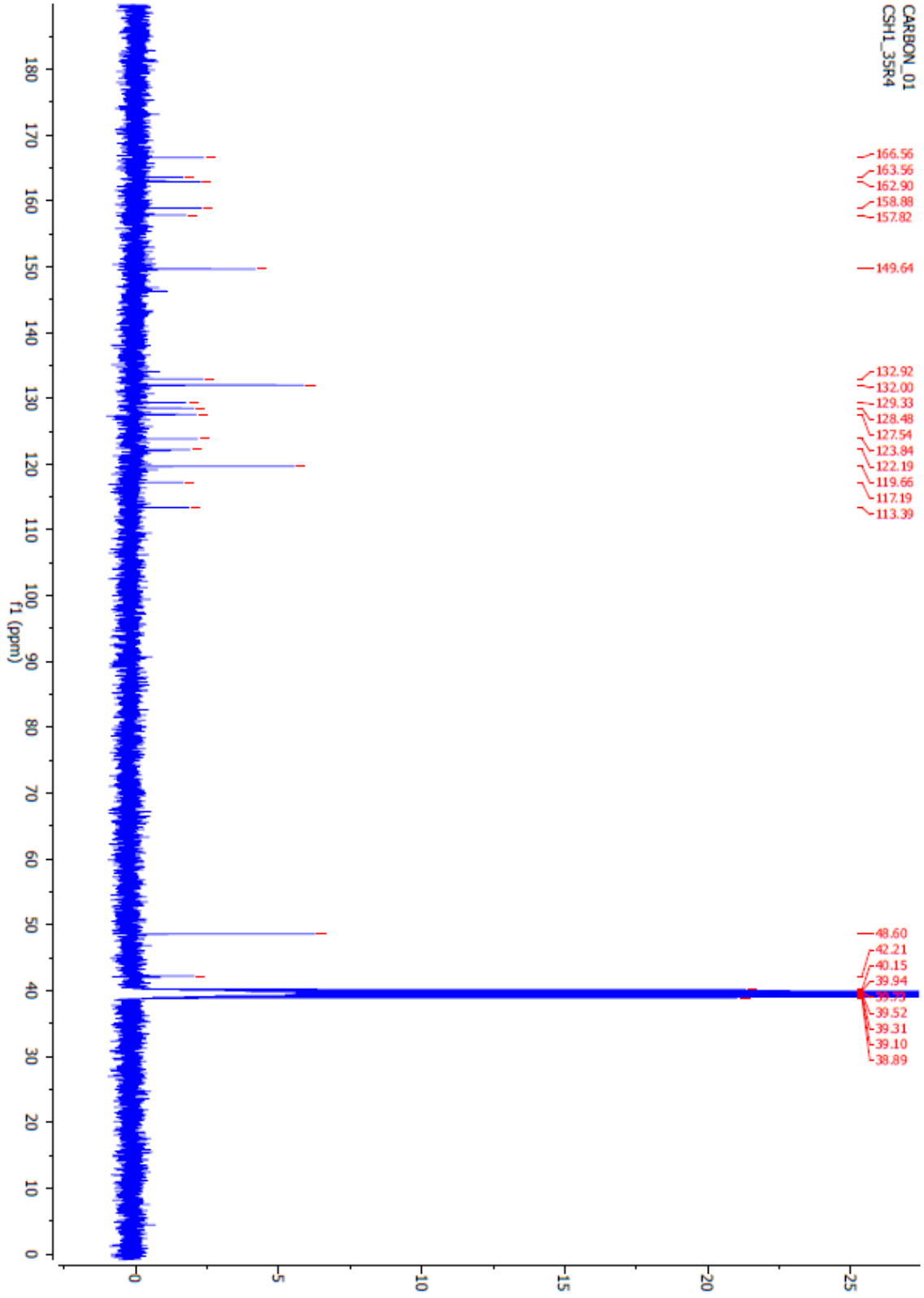

Figure S17 ^{13}C NMR spectrum of **HL** (400MHz, d_6-DMSO)

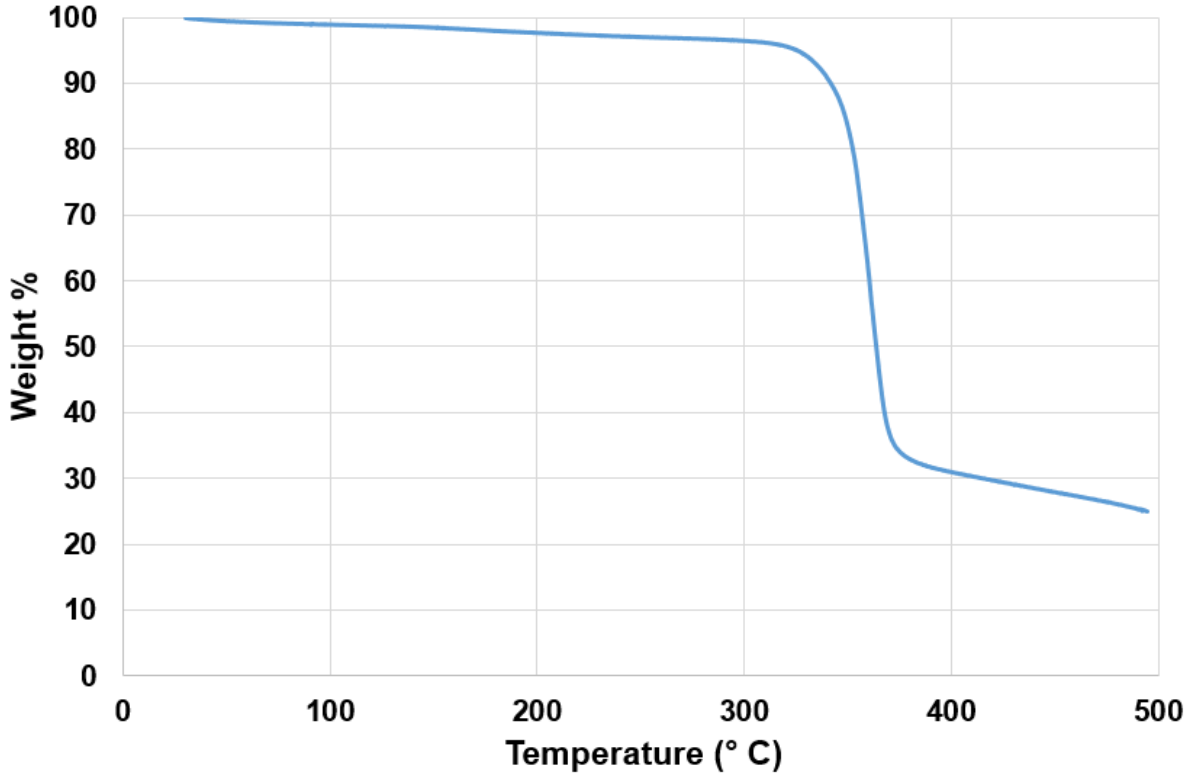

Figure S18 Thermogravimetric analysis of **HL**·0.66H_2O. The total mass loss in the range 30 – 250 °C prior to the onset of decomposition is 2.9% (calculated for **HL**·0.66H_2O 2.8%).

References

S1 A. L. Spek, *Acta Crystallogr., Sect. C: Struct. Chem.* 2015, **71**, 9-18.

S2 C. S. Hawes, K. Byrne, W. Schmitt and T. Gunnlaugsson, *Inorg. Chem.* 2016, **55**, 11570-11582.

S3 J. I. Lovitt, C. S. Hawes, A. D. Lynes, B. Haffner, M. E. Möbius and T. Gunnlaugsson, *Inorg. Chem. Front.* 2017, **4**, 296-308.

S4 B*ruker APEX-3*, Bruker-AXS Inc., Madison, WI, 2016.

S5 *SADABS*, Bruker-AXS Inc., Madison, WI, 2016.

S6 G. M. Sheldrick, *Acta Crystallogr. Sect. A*, 2015, **71**, 3-8.

S7 G. M. Sheldrick *Acta Crystallogr. Sect. C*, 2015, **71**, 3-8.

S8 O. V. Dolomanov, L. J. Bourhis, R. J. Gildea, J. A. K. Howard and H. Puschmann, *J. Appl. Crystallogr.*, 2009, **42**, 339-341.

S9 Horiba Scientific, "A Guide to Recording Fluorescence Quantum Yields", http://www.horiba.com/scientific/products/fluorescence-spectroscopy/application-notes/quantum-yields/; accessed 7/8/2016.

S10 A. M. Brouwer, *Pure. Appl. Chem.* 2011, **83**, 2213-2228.